A Remote Anomaly Detection System for Slocum Underwater Gliders

Enrico Anderlini[a,*], Georgios Salavasidis[b], Catherine A. Harris[b], Peng Wu[a], Alvaro Lorenzo[b], Alexander B. Phillips[b], Giles Thomas[a]

[a] *Department of Mechanical Engineering, Roberts Building, University College London, Torrington Place, London, WC1E 7JE, UK*

[b] *Marine Autonomous and Robotic Systems, National Oceanography Centre, European Way, Southampton, SO14 3ZH, UK*

Abstract

Marine Autonomous Systems (MAS) operating at sea beyond visual line of sight need to be self-reliant, as any malfunction could lead to loss or pose a risk to other sea users. In the absence of fully automated on-board control and fault detection tools, MAS are piloted and monitored by experts, resulting in high operational costs and limiting the scale of observational fleets that can be deployed simultaneously. Hence, an effective anomaly detection system is fundamental to increase fleet capacity and reliability. In this study, an on-line, remote fault detection system is developed for underwater gliders. Two alternative methods are analysed using time series data: feed-forward deep neural networks estimating the glider's vertical velocity and an autoncoder. The systems are trained using field data from four baseline deployments of Slocum gliders and tested on six deployments of vehicles suffering from adverse behaviour. The methods are able to successfully detect a range of anomalies in the near real time data streams, whilst being able to generalise to different glider configurations. The autoencoder's error in reconstructing the original signals is the clearest indicator of anomalies. Thus, the autoencoder is a prime candidate to be included into an all-encompassing condition monitoring system for MAS.

Keywords: fault detection, anomaly detection, underwater gliders, autonomous underwater vehicles, autoencoder, deep learning, system identification

*Principal corresponding author

Email address: E.Anderlini@ucl.ac.uk (Enrico Anderlini)

Nomenclature

α	angle of attack [°]
α_T	glider thermal expansivity [$°C^{-1}$]
β	glide-path angle [°]
$\ddot{z}$	vertical acceleration in the inertial frame [cm/s^2]
δB	buoyancy offset [N]
δ_r	rudder angle [°]
$\dot{\delta}_\mathrm{r}$	rate of change of rudder angle [°/s]
$\dot{\phi}$	roll angular velocity [°/s]
$\dot{\psi}$	yaw angular velocity [°/s]
$\dot{\theta}$	pitch angular velocity [°/s]
$\dot{V}_\mathrm{vbd}$	rate of change of VBD volume [cm^3/s]
$\dot{x}_\mathrm{b}$	rate of change of battery position [cm/s]
$\dot{z}$	vertical velocity in the inertial frame [cm/s]
ϵ_c	glider absolute compressibility [$dbar^{-1}$]
ϕ	roll angle [°]
ρ	water density [kg/m^3]
θ	pitch angle [°]
$\tilde{\psi}$	yaw angle [°]
f_1	engineered feature [kg]
f_2	engineered feature [kg]
g	gravitational acceleration [m/s^2]
m	glider flooded mass [kg]

p	water pressure [dbar]
S	glider wetted surface area [m^2]
T	water temperature [°C]
T_0	reference temperature [°C]
V_0	glider reference volume [m^3]
V_{vbd}	Variable Buoyancy Device (VBD) volume [cm^3]
x_{b}	battery position [cm]
z	vertical position in the inertial frame [m]

1. Introduction

1.1. Background and Motivation

The pervasive adoption of Marine Autonomous Systems (MAS) is currently constrained by the challenges of operating fully independently of support vessels, in the demanding dynamic environment of the world's oceans. MAS are piloted and monitored by experts, keeping operational costs high and limiting the scale of observational fleets that can be deployed simultaneously (Verma and Simmons, 2006). Since a MAS can be at sea for months at a time, operating 'over-the-horizon' from human pilots and support vessels, it is impossible to perform reactive maintenance, i.e. maintenance when a fault occurs. Therefore, strategies must be developed for automated fault diagnostics and prognostics in a predictive maintenance framework, i.e. identifying when maintenance should be preemptively scheduled on individual components, by continuously monitoring conditions and MAS behaviour during operation. Current manual detection, diagnosis and mitigation of problems are limited by the experience of the individual pilot and are subject to human error, especially when a MAS platform requires pilot attention around the clock.

In the absence of general on-board anomaly detection and diagnosis systems, the ability to transmit sensor data in a timely manner to an off-board system or human operator and to receive appropriate commands in response becomes of critical importance for MAS safety and performance.

Anomaly detection is currently extremely challenging for Autonomous Underwater Vehicles (AUVs), as they are under-observed systems, with limited or decimated data available via satellite for pilots to interpret when the vehicle comes periodically to the surface. If the underlying cause of observed adverse behaviour cannot be correctly diagnosed and the situation remedied (e.g. via the remote adjustment of piloting parameters or mission scope), the vehicle, their cargo or data can be lost or present a hazard to shipping (Thieme and Utne, 2017).

1.2. Literature Review

Underwater Gliders (UGs) are a type of AUV that are being used extensively for long-term observation of key physical oceanographic parameters (Rudnick, 2016). The vehicles achieve vertical motion in the water column by changing their buoyancy through a variable buoyancy device (VBD). Wings generate a forward motion component from the vertical motion. Hence, UGs travel in a characteristic sawtooth pattern in the vertical plane. Their simple propulsion system, which consists of the VBD, pitch control and either roll control or a rudder, is highly efficient. Therefore, although they operate at a low surge speed (≈ 0.3 m/s), the deployments of UGs can last for several months. Reviews of the initial glider technologies can be found in Davis et al. (2003) and Wood (2009), whilst Rudnick (2016) and Testor et al. (2019) contain good summaries of their applications in oceanography.

The reliability of UGs is analysed thoroughly in Brito et al. (2014), with the authors collecting failure data from most European operators. The most common failures have been observed to be leakages, failures of electrical (e.g. the battery, satellite communication hardware), mechanical components (e.g. the VBD pump and bladder, rudder and roll motor), navigation and scientific sensors, and software errors. Leaks, motor or pump malfunctions, low-battery voltage and sensor drop-outs or faults are also identified as problems in Schofield et al. (2007) Additionally, Frajka-Williams et al. (2011) have observed the failure of the pitch tilt sensor. Furthermore, the authors have investigated the loss of wing for UGs in Anderlini et al. (2020a) and the impact of biofouling in Anderlini et al. (2020b).

Methods for fault detection and diagnostics can be subdivided into rule-based, model-based and data-driven solutions (Hamilton et al., 2007).

Rule-based methods rely on bespoke heuristics, usually in the form of if-then statements, obtained from designers' observations of the system. Model-based approaches rely on dynamic models of the physical systems. Hence,

model-based methods are highly suitable for condition monitoring of new systems where available data is limited. Model-based techniques are robust, simple and relatively inexpensive computationally, but multiple systems are usually run concurrently for redundancy. Specifically for AUVs, Freddi et al. (2013) design a system to detect faulty thrusters. Hamilton et al. (2007) propose an integrated fault detection and diagnosis architecture for AUVs, although the focus is on on-board systems.

Data-driven solutions rely on the analysis of actual sensor data, thus showing significant improvements in accuracy when large data sets are available. In particular, deep-learning-based methods can be generalised to different applications and can be scaled to a large number of sensors, but need many samples for training.

Data-driven condition monitoring solutions, with a focus on machine and deep learning, are surveyed in Ellefsen et al. (2019) for autonomous ships, with (Fink et al., 2020) providing an overview of present and current trends in data-driven fault diagnostics and prognostics. Specifically for AUVs, data-driven fault detection methods include radial basis function networks (Wang and Zhang, 2006), Gaussian particle filter (Sun et al., 2016) and artificial immune system (Yao et al., 2018). Raanan et al. (2018) have introduced an automatic fault detection system for long-range AUVs based on Bayesian nonparametric topic modelling techniques. Although the data set focuses on the identification of bottoming events, the behaviour of the analysed long-range AUV is similar to that of UGs. A system to develop safety indicators for the operation of MAS is described in Thieme and Utne (2017), with a case study on an AUV. An anomaly detection system for UGs specific to marine biofouling was presented in Anderlini et al. (2021) using ensembles of regression trees and K-means clustering.

Modern deep learning solution specific to anomaly detection are summarised in Pang et al. (2021). Of the three main deep anomaly detection paradigms, learning the feature representations of normality is of interest for the UG application, i.e. being able to differentiate between normal and abnormal operating conditions with anomaly scoring. These methods can be further subdivided into generic feature learning and anomaly measure-dependent feature learning. Whereas the latter aims at learning feature representations that are optimised for one specific existing anomaly measure, the former is more general and can deal well with imbalanced datasets heavily skewed towards normal operating conditions due to the low anomaly detection recall rate. Autoencoders are a very powerful, but simple strat-

egy that consists of a network that learns to reconstruct the original signals passing through a smaller latent space that summarises only the fundamental information removing the effect of noise. Their generality makes them well suited for the application to UGs. An alternative modification specific to UGs consists of reconstructing only the vertical velocity signal based on the other sensors. This procedure is similar to the model-based anomaly detection strategies (Anderlini et al., 2020a), but with a model with many more parameters. In particular, the difference between a machine learning implementation that relies on engineered features from the dynamic model and a deep learning strategy that relies only on the raw variables should be investigated.

1.3. Contribution

The operation of MAS platforms beyond visual line of sight requires a suitable command and control system. For example, the UK National Oceanography Centre are designing a new command-and-control system for efficient MAS fleet management (Farley et al., 2019; Harris et al., 2020) to facilitate the over-the-horizon operation of their ever-increasing fleet of AUVs. Another example is the LSTS Neptus and Dune over-the-horizon command-and-control environment (Sousa Dias et al., 2005; Madureira et al., 2013; Pinto et al., 2013) Control and command systems will require an effective condition monitoring tool to enable round-the-clock operations. Rule-based and model-based over-the-horizon fault detection methods have been introduced for UGs in Anderlini et al. (2020a) and Anderlini et al. (2020b) for specific faults, namely wing loss and marine growth. However, more general solutions are required.

This work introduces the first data-driven fault detection system for UGs. In particular, two alternative methods are investigated: an autoencoder extracting useful features in a latent space, and a deep neural network (DNN) regression approach estimating the UG's vertical velocity. The systems are trained with the steady-state flight data from four deployments of healthy Slocum UGs and tested on six deployments of Slocum UGs suffering from adverse behaviour. The performance of the data-driven methods is assessed against existing rule- and model-based solutions (Anderlini et al., 2020a,b) to show the improvement in generality.

1.4. Article Organisation

In Section 2.1, the operations of Slocum UGs and the analysed datasets are described. The novel data-driven anomaly detection methods are introduced in Section 3. Then, the results are presented and discussed in Section 4, with concluding remarks being made in Section 5.

2. Slocum Gliders Data

2.1. Slocum Underwater Gliders

There are range of manufacturers of underwater gliders (Rudnick, 2016). This study is focused on 200m depth rated Slocum G2's from Teledyne Webb Research (Webb et al., 2001; Schofield et al., 2007). An example can be seen in Fig. 1.

As shown in Fig. 2, the Slocums are actuated by a VBD, which consists in an oil bladder that can be extended or retracted from the pressure hull. When the bladder is outside the pressure hull, the vehicle's displacement increases and so does its net buoyancy and vice versa, resulting in their characteristic 'yo-yo' motion. The vehicles considered in this study are limited to changes in the VBD volume of ± 250 cm^3. Furthermore, pitch is controlled by shifting the position of one movable battery pack with a dedicated mechanism. Yaw is controlled via a rudder, which is magnetically coupled to a servo motor to avoid an opening in the pressure hull.

Example time series data for a typical dive cycle can be seen in Fig. 3. z indicates the vertical position of the vehicle in the water column (positive upwards), which is measured by an on-board pressure sensor. Its time-derivative yields $\dot{z}$, the vertical velocity. The actuators' control signals are the volume of the VBD, V_{vbd}, the position of the moving battery pack, x_{b}, and the rudder angle, δ_{r}. The roll, ϕ, and pitch, θ, angles are measured by tilt sensors, while a magnetic compass indicates the heading angle, ψ. In this article, the difference of the instantaneous yaw angle and the mean yaw angle over the whole dive cycle, $\bar{\psi}$, is used to favour the body-fixed over the inertial reference frame.

As shown in Fig. 2 and Fig. 3a, Slocums can perform multiple 'yos' per dive (two in this particular case). This means that the vehicle can sample the water column multiple times before returning to the surface to send and receive data by satellite and get a new position fix via GPS (Teledyne Webb Research, 2012). The data sent ashore needs to be decimated to reduce the time that the vehicle spends on the surface to lower a) the risk of damage

Figure 1: Slocum G2 operated by the NOC.

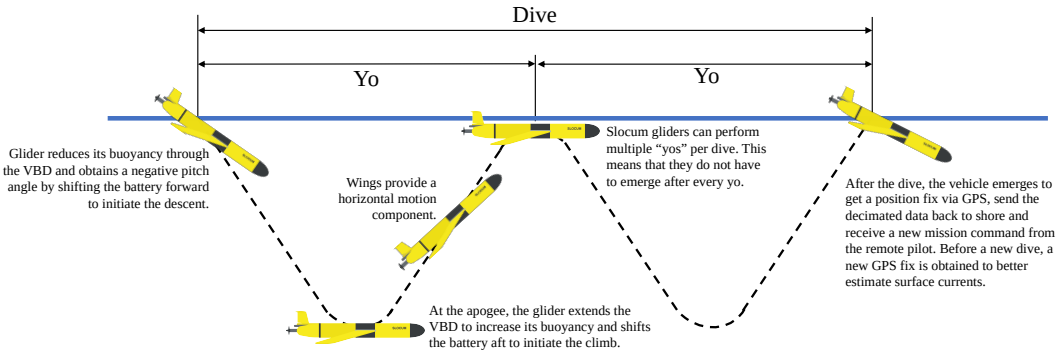

Figure 2: Diagram showing the concept of operation of a Slocum UG. The drawing is not to scale: the analysed vehicles reach their apogee at 200-m-depth and and have glide path angles with a magnitude in the range $(15°, 30°)$.

from collisions with other sea users and wave loads, b) the power expenditure and c) the actual financial cost associated with the transmission of the data by satellite (specifically, via Iridium). The data usually includes the vehicle's orientation, its depth (from which the vertical velocity can be obtained), the actuator's signals, the capacity and voltage of the battery, the estimated position, samples of the scientific data of interest and warnings from on-board health monitoring systems. The decimation means that the samples have a

low rate, typically with a time step of 30-60 s for signals that are considered of least importance (e.g. the roll angle) and 10 s for the signals that are of most interest, e.g. the scientific data. In the analysed data sets, each dive consisted of up to 14 yos and lasted up to four hours.

Fig. 3b, Fig. 3c and Fig. 3e show the control input and output for the VBD, battery linear actuator and rudder. From a comparison with Anderlini et al. (2019b), it is possible to notice that the rudder enables Slocums to exhibit a much smoother response than other UG technologies, even for shallower dives where disturbances are stronger. In Fig. 3c, it is also interesting to note that the direction of travel of the battery is opposite to the pitch angle, which is due to the actuator's reference frame.

To control UGs, pilots rely on the surface dialogue, with a user-friendly interface providing information on the vehicle's health status, current mission plan, last GPS position and the decimated data from past dives. Typically, during normal operation, the remote pilots will first check the surface dialogue for errors, warning and oddities from the glider, along with the dive profile to ensure it is symmetrical and the glider is reaching the target depth. The most common errors identified on-board are relatively mild aborts, e.g. glider stalls, behaviour errors, and communication interruptions (Schofield et al., 2007). Progress towards the target waypoint is also considered, along with a check of the battery health and consumption. This full check is usually performed once per day, with the pilot making smaller observations more regularly after each dive. Therefore, pilots are only likely to look into the flight parameters in detail if the glider is reporting errors, is failing to dive correctly or is not making progress towards a waypoint. Hence, issues with roll, for instance, can go unnoticed.

2.2. Dataset Description

This study uses the data measured by Slocum G2 gliders over ten deployments operated by the NOC (BODC, 2021). A summary of the missions, including unit (or UG) ID, mission date and location, can be found in Table 1. As can be seen, the vehicles were operated in either the Celtic or North Seas between 2014 and 2019.

The missions in the Celtic Sea were run as part of project AtlantOS (EC/633211), with the work extended and complemented by project CaNDyFloSS: 'Carbon and Nutrient Dynamics and Fluxes over Shelf Systems' (NE/K001701/1). The project relied on multiple deployments of UGs to test

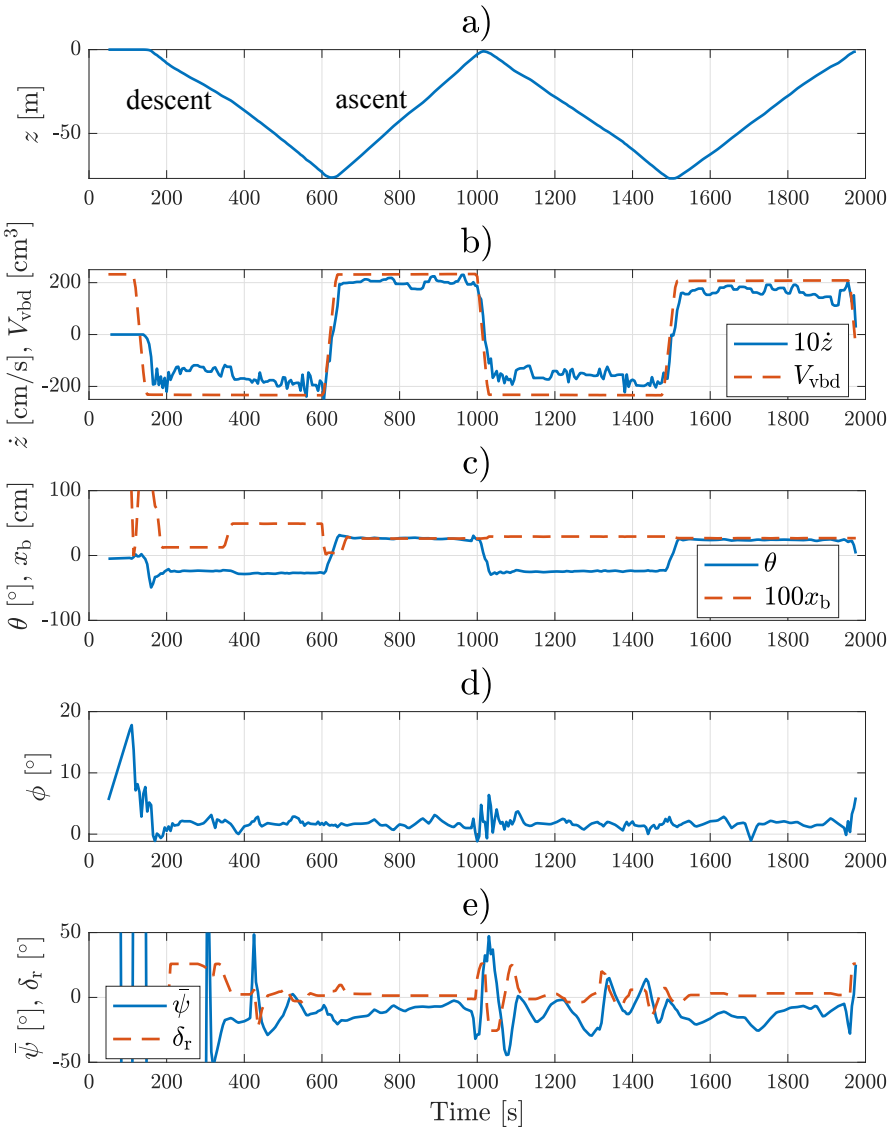

Figure 3: Example dive cycle of an intact Slocum glider.

the capability of MAS to synoptically assess physical and biogeochemical functioning in shelf sea systems (Palmer et al., 2018).

The missions in the North Sea were part of project ALTERECO: "An Alternative Framework to Assess Marine Ecosystem in Shelf Seas" (NE/P013902/2). In this project, the UGs were used to validate a novel monitoring framework

Table 1: Summary of the analysed deployments (BODC, 2021), including the hydrostatics of the UGs.

No.	**Unit**	**Date**	**Location**	**Duration [days]**	m [kg]	V_0 [cm^3]	T_0 [°C]
1	345	2014	Celtic Sea	123.9	58.863	57398.8	19.98
2	345	2019	North Sea	76.8	64.587	63017.6	19.64
3	397	2015	Celtic Sea	45.9	59.400	57990.4	15.90
4	419	2015	Celtic Sea	11.0	65.236	63682.0	15.88
5	194	2017	North Sea	83.9	58.631	57226.0	20.83
6	399	2015	Celtic Sea	84.6	65.258	63665.8	16.80
7	423	2015	Celtic Sea	6.8	65.850	64303.2	16.13
8	424	2015	Celtic Sea	20.8	66.026	64435.3	16.13
9	304	2019	North Sea	76.9	59.044	57615.8	19.23
10	436	2019	North Sea	89.8	65.281	63716.5	19.45

to deliver improved understanding in time and space shelf sea ecosystem health and functioning (Matthew R. Palmer et al., 2020).

Gliders were deployed and recovered from a mixture of large and small research vessels as well as fishing boats. Once deployed, gliders undertook sustained observations for multi-month periods, undertaking repeated transects in the relevant operating area. The only human intervention was via remote pilots, up until the point of recovery. By cycling the gliders sustained observations can be extended to multiple years.

3. Anomaly Detection

Here, a novel data-driven anomaly detection system for UGs is developed to identify adverse behaviour over the horizon, as summarised schematically in Fig. 4. The method is developed and tested off-line using the deployment data sets shown in Table 1. The system is trained using baseline data from deployments where the vehicle exhibited healthy status and tested with deployments datasets exhibiting adverse vehicle behaviour. Once the efficacy of the system is established, the trained anomaly detection schemes can be used on-line from the remote control centre to notify pilots of possible faults with the UG after each surfacing and satellite connection, as shown in Fig. 2. It is important to note that vehicles store on-board all data samples, whilst they send by satellite only decimated data due to the associated cost and power loss. Hence, the training data can be subjected to deeper cleaning than the decimated real-time data.

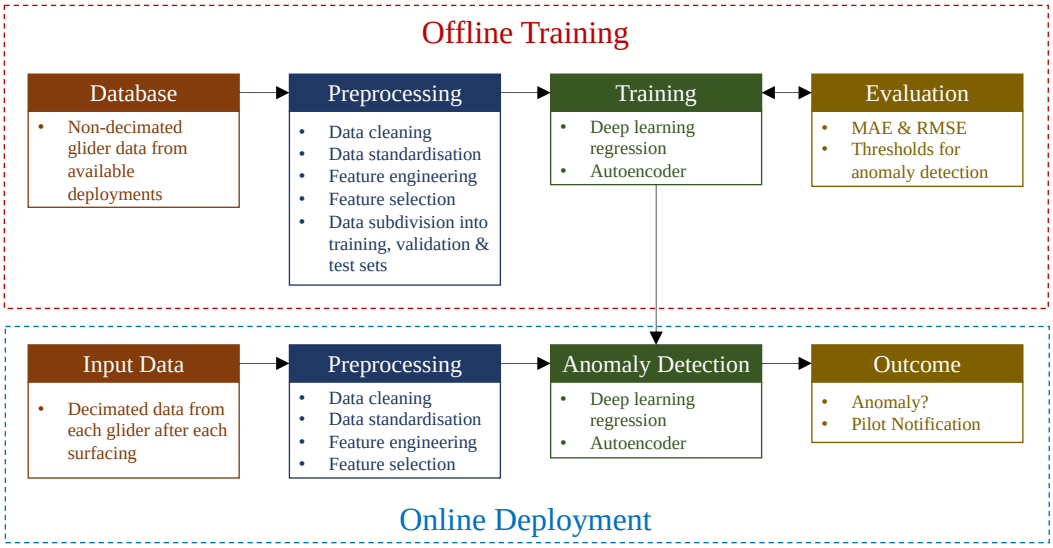

Figure 4: Diagram of the new fault detection system for Slocum underwater gliders.

Two alternative data-driven solutions are investigated: an autoencoder extracting useful features in a latent space, and a deep neural network (DNN) regression approach estimating the UG's vertical velocity. In the following sections, the preprocessing step and the development of the individual fault detection schemes are treated in detail.

3.1. Steady-State Flight Model of a UG

As described in Sec. 2.1, UGs operate in steady-state conditions for most of the descent and ascent of each yo. The free-body diagram of the equilibrium condition for the steady-state flight is shown schematically in Fig. 5a and Fig. 5b for descents and ascents, respectively. B indicates the net buoyancy, L the lift and D the drag force. U is the surge velocity component in the body-fixed frame, θ the pitch, α the attack and β the glide-path angles. The glide-path angle indicates the angle of the flight path in the inertial reference system and is obtained from the sum of the pitch and attack angles: $\beta = \theta + \alpha$.

In both descents and ascents, the balance of forces in equilibrium resulting in steady state flight yields (Merckelbach et al., 2019)

$$B - L\cos\beta - D\sin\beta = 0. \tag{1}$$

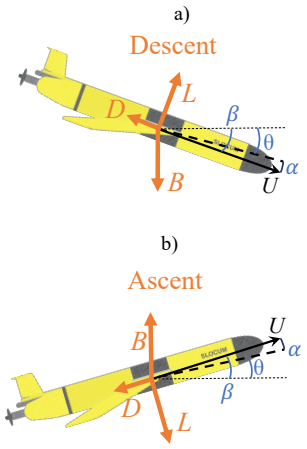

Figure 5: Free-body diagram of the intact glider in dives (a) and climbs (b) (profile view).

This persists over the majority of a dive cycle. The drag and lift forces can be modelled as

$$L = \frac{1}{2} k_{\mathrm{L}} \alpha \rho S U^2, \tag{2}$$

$$D = \frac{1}{2} \left(k_{\mathrm{D},0} + k_{\mathrm{D,L}} \alpha^2 \right) \rho S U^2, \tag{3}$$

where ρ is the water density, S is the wetted surface area, k_{L}, $k_{\mathrm{D},0}$ and $k_{\mathrm{D,L}}$ are constants used to compute the lift, drag and induced drag coefficients. The water density is obtained from the water pressure, salinity and temperature (and the derived conductivity) using the Gibbs Seawater Toolbox (McDougall and Barker, 2011). These properties are measured by a Conductivity, Temperature and Density (CTD) sensor.

The net buoyancy force can be computed as

$$B = g \left\{ -m + \rho \left[V_0 \left(1 - \epsilon_c p + \alpha_T (T - T_0) \right) + V_{\mathrm{vbd}} \right] \right\} + \delta B, \tag{4}$$

where g is the gravitational acceleration, m is the UG mass, V_0 its reference volume, ϵ_c the absolute compressibility of the pressure hull and α_T its thermal expansivity, with the reference temperature T_0. p is the water pressure and T its temperature. The offset in buoyancy δB is added to account for possible changes in the net buoyancy of the vehicle after faults.

3.2. Preprocessing

3.2.1. Data Cleaning

As UGs are in steady-state flight for most of their deployment, the development of data-driven anomaly detection strategies can be greatly simplified. However, data cleaning is necessary to discard transient effects. In this study, the recovery-mode data stored on-board the gliders in the .DBD and .EBD files is used for the training and evaluation of the fault dection schemes (Teledyne Webb Research, 2012). The data is converted from binary to ASCII format using the Python *dbdreader* module[1]. Subsequently, the points are imported into the MATLAB environment.

Due to the large size of the available datasets (more than 8 million points for all combined deployments), all dive cycles for which any of the signals of interest are unavailable are removed. Additionally, a time vector starting from 0 s is created for every cycle. In a further cleaning sweep, all cycles with either a maximum depth shallower than 25 m or less than 10 time stamps are removed.

The greatest challenge for the cleaning process is represented by the time synchronisation: all sensors sample at slightly different time stamps. Furthermore, the navigation and scientific (for the CTD) Central Processing Units (CPUs) are synced only at the surface, so that a time drift is noticeable (with a mean drift of 3 s over 4 hr). Hence, all signals are resampled by linear interpolation for exactly the same time stamps, with a time step of 5 s. The navigation and scientific computers are synced through the pressure signal, which is measured by both units.

Afterwards, the variables of interest, such as vertical velocity and water density, are computed from the raw signals. Furthermore, the signals are modified to reflect the units shown in the nomenclature. Additionally, the data is split into individual yo and their dive and climb stages. In Fig. 3b, the vertical velocity signal is noisier than the VBD volume signal. Hence, changes in sign of the difference between values of V_{vbd} for neighbouring time stamps are used to identify individual dives and climbs.

To reduce the transient effects caused by operations on the surface and apogee, points within 15 m from the surface (or the highest point of the climb) and the maximum depth are ignored. Furthermore, only steady-state data are kept by removing points which present significant changes in the

[1] https://pypi.org/project/dbdreader/

Table 2: Upper limits used in the data cleaning.

Variable	**Upper Limit**
$\lvert\ddot{z}\rvert$	5 cm/s^2
$\lvert\dot{\phi}\rvert$	0.2°/s
$\lvert\dot{\theta}\rvert$	0.2°/s
$\lvert\dot{\psi}\rvert$	0.5°/s
$\lvert\dot{V}_{\mathrm{vbd}}\rvert$	0.05 cm^3/s
$\lvert\dot{x}_{\mathrm{b}}\rvert$	0.01 cm/s
$\lvert\dot{\delta}_{\mathrm{r}}\rvert$	2°/s

actuators' values, high vertical acceleration or high rotational velocities, as shown in Table 2. All points which present a non-numeric value for any signals are removed. The data are then merged once again for each cycle and any empty cells at this stage are cleared.

3.2.2. Data Standardisation, Feature Selection and Engineering

For the data-driven strategies, using the data values expressed in the physical units may result in bias towards values with much higher mean or standard deviation values, e.g. the VBD volume. Hence, for these data-based solutions, the input data is standardised (Goodfellow et al., 2016), as this has been found to be more effective than normalisation for this particular case.

Feature selection and engineering are specific to each method and will thus be covered in the following individual sections.

3.3. Deep Learning for Vertical Velocity Prediction

Machine and deep learning strategies are increasingly being used for condition monitoring applications (Fink et al., 2020). Similarly to the model-based diagnostics, the error between the predicted and actual vertical velocity can be used to indicate anomalies. Hence, for UGs it is possible to simplify the anomaly detection system to the tracking of the loss of the predicted vertical velocity in steady-state flight. The system can then be trained using data coming from deployments representing healthy baseline conditions. By tracking the prediction error, which is expected to rise for damaged gliders, it is possible to identify faults. Limiting the analysis to steady-state data greatly reduces the complexity of the problem, as simpler feedforward DNNs

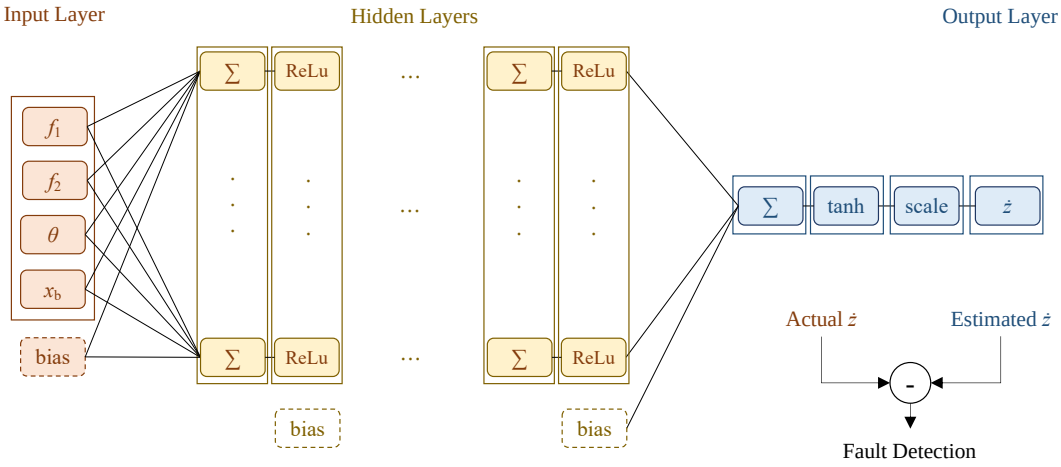

Figure 6: Diagram of the ANN used for fault detection for UGs.

may be used instead of more complex recurrent or convolutional architectures (Fink et al., 2020).

LeCun et al. (2015) define a deep neural network as a network with more than one hidden layer. However, other than training algorithms and activation functions, the main difference between classical machine learning and deep learning consists in the size of the dataset analysed (Goodfellow et al., 2016). Machine learning algorithms require significant levels of feature engineering and their performance does not improve after a specific dataset size. With deep learning solutions, even raw signals can be directly used as features. Deep learning solutions are better scalable, thus presenting much higher prediction accuracy than conventional machine learning strategies for extremely large datasets (i.e. with more than approximately 10^6 points).

Here, two neural networks are considered and will be labelled as artificial neural network (ANN) and deep neural network (DNN) despite both of them having more than one hidden layer. Both will analyse the same cleaned data as for the dynamic model. However, while for the ANN additional feature engineering is performed, the DNN relies on the unmodified features.

From the dynamic model, the features of interest to predict the vertical velocity of the vehicle are identified to be the VBD volume, the pitch angle, the battery position, the water density, pressure and temperature. Hence,

the following two engineered features are obtained for the ANN:

$$f_1 = V_{\text{vbd}}\rho, \tag{5a}$$

$$f_2 = \rho V_0 \left(1 - \epsilon_c p + \alpha_T (T - T_0)\right). \tag{5b}$$

The first feature, f_1, is expected to be dominant. To understand whether the second feature, f_2, should also be selected, a hypothesis test is run on the root mean square error (RMSE) values of the test set for the ANN both with and without f_2 to assess whether the results are statistically different. Firstly, the Lilliefors test is run to check whether the RMSE values are normally distributed. As the error distribution does not belong to the normal family, the non-parametric Wilcoxon signed rank test is used to assess whether the difference of the two distributions has zero median. For both hypothesis tests, a significance value of 5% is employed (Gibbons and Chakraborti, 2011). The results of the tests can be found in Section 4.3.

Additionally, the training set of the standardised data is subdivided into training, holdout and test sets in the following proportions: 85%, 10% and 5%. The training set contains examples used to fit the model parameters during learning. The holdout set is employed to tune hyperparemeters during training. The test set enables an evaluation of the final, fully trained system (Goodfellow et al., 2016).

The neural networks used for the fault detection are shown in Fig. 6 and Fig. 7, respectively. To detect faults, the RMSE and mean absolute error (MAE) of the predicted vertical velocities as compared with the actual measured $\dot{z}$ are tracked. Both networks have a number of hidden layers with a number of neurons that needs to be optimised. Whilst the hidden layers have ReLu activation functions (Goodfellow et al., 2016), the output layer has a hyperbolic tangent activation function. The Adam optimisation algorithm is used for training (Kingma and Ba, 2015), with L_2 regularisation to avoid overfitting and using the loss (or MAE) to assess convergence (Goodfellow et al., 2016).

3.4. Autoencoder

Autoencoders are a successful unsupervised learning strategy for fault detection (Reddy et al., 2016; Fink et al., 2020). An autoencoder is a DNN that comprises a dimensionality reduction step followed by a data reconstruction step. The input and output features are thus identical for the autoencoder. By compressing and reconstructing the data, the autoencoder is able to learn

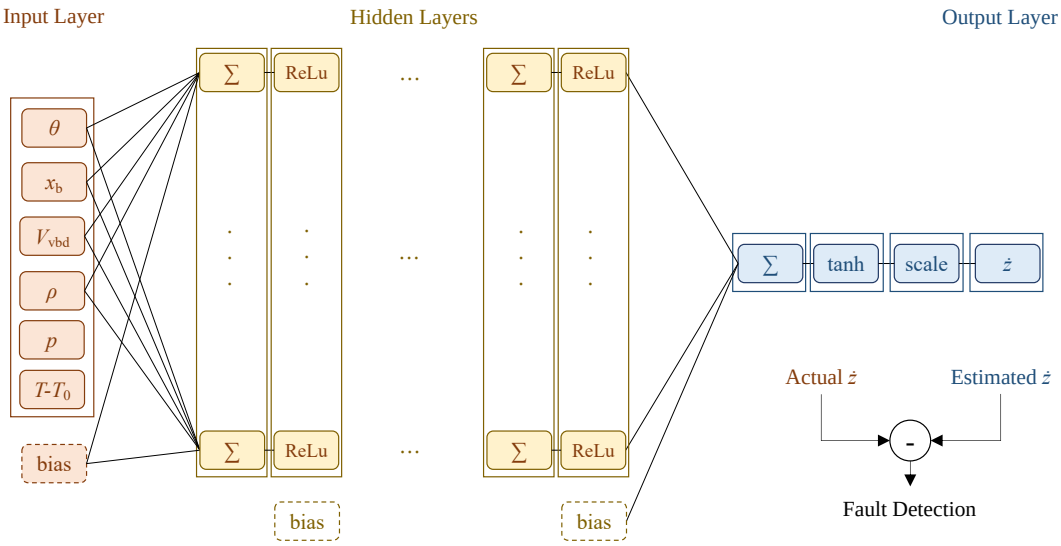

Figure 7: Diagram of the DNN used for fault detection for UGs.

a low-dimensional representation by identifying correlated variables and ignoring signal noise (Goodfellow et al., 2016). For fault detection, training the autoencoder on a dataset of a fully operational system enables the identification of anomalies by tracking the autoencoder error in its reconstruction of the baseline features.

For the anomaly detection system for UGs, the autoencoder shown in Fig. 8 is adopted. The selected features are the vertical velocity, the product of the VBD volume and the water density, the pitch angle and the battery position. Adding the water temperature and pressure was found to cause high levels of noise with little benefit on the overall prediction. Adding the roll angle would cause the response of the autoencoder at predicting anomalies to improve. However, the roll tilt sensor is not fundamental for the operation of the vehicle. Hence, it has been preferred to only use signals fundamental for the operation of the UGs in the autoencoder.

As only four features are used, a single hidden layer is sufficient. To select the number of hidden neurons, a principal component analysis (PCA) (Jollife and Cadima, 2016) is run. Both hidden and output neurons present a hyperbolic activation function. The scaling layer in the output layer is required because the output data (like the input) is standardised rather than normalised, i.e. it goes beyond the range $(0, 1)$. By tracking the average

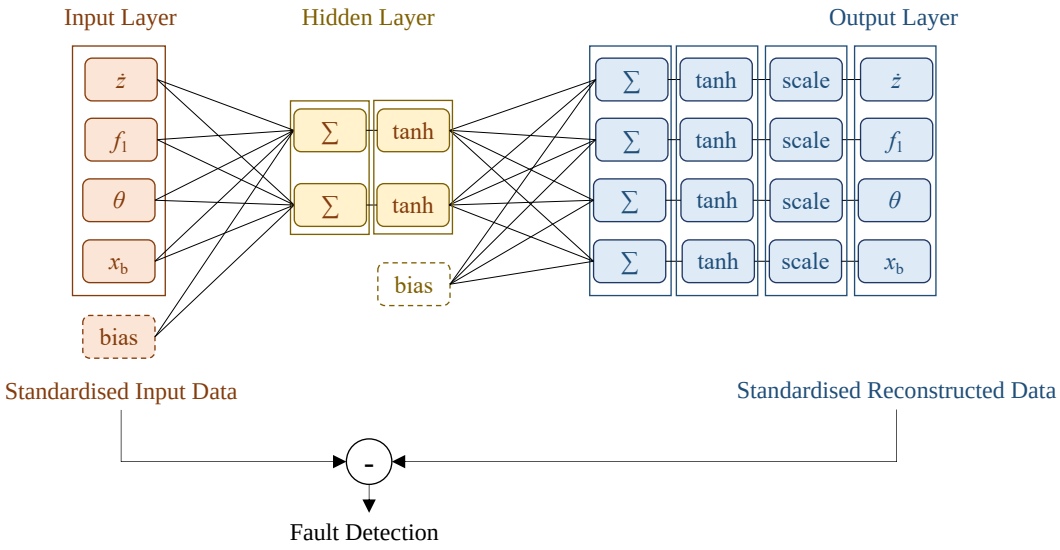

Figure 8: Diagram of the autoencoder used for fault detection for UGs.

RMSE of the prediction of the output features, it is possible to identify anomalies.

Similarly to the DNNs, the training data set is subdivided into training, holdout and test sets in the following proportions: 85%, 10% and 5%. The Adam optimisation algorithm is used for training (Kingma and Ba, 2015), with L_2 regularisation to avoid overfitting and using the loss (or MAE) to assess convergence (Goodfellow et al., 2016). Most often the Kullback-Leibler divergence is employed, especially in image recognition tasks (Goodfellow et al., 2016), but here the selected architecture has been found to be particularly effective.

4. Results and Discussion

In this section, the deployment data is firstly analysed and visualised to gather insights into the UG dynamics. From this study, the data from specific deployments is selected for the training and testing of the deep learning solutions. Finally, the performance of the new anomaly detection system is discussed.

4.1. Data Averaged over each Dive Cycle

Figures 9-11 show the variation in the mean vertical velocity, VBD volume, pitch angle, battery position, roll, and rudder angles with mission duration for all Slocum UGs in the study only up to 80 days after the start of each deployment. The yaw angle is not shown, as its signal is very noisy due to ocean currents.

From Fig. 9-11, the following observations can be made of the deployments:

- Unit 345 (2014 deployment) presents a significant gap in the data, which may have been caused by retrieval and reset at sea.

- Unit 345 (2019 deployment) exhibits interesting changes in roll of small magnitude throughout the mission probably due to strong disturbances, such as transverse ocean currents.

- Unit 194 presents an abrupt change in vertical velocity, VBD volume, pitch angle and battery position for the last few dive cycles (Fig. 9-10). As the changes affect all variables in the correct direction, this effect is possibly to be due to the pilot's decision.

- Unit 194 presents a significant angle of list of approximately 9°. The list angle can be identified in Fig. 11, as the roll angle has the same value in descents and ascents. Although the high roll angle may be caused by a sensor failure, which can happen on UGs (Brito et al., 2014), the corresponding rudder angle with an opposite sign indicates the effect is real. The UG is compensating for the list angle and thus asymmetric drag and lift forces with a constant rudder angle, which causes additional parasitic drag and thus energy expenditure.

- Unit 399 shows a decrease in the magnitude of the vertical velocity with time in both descents and ascents despite an increase in VBD volume in climbs. This behaviour is likely to be associated with marine growth (Haldeman et al., 2016), although no evidence of this is available from the records.

- Units 423 and 424 present much greater input VBD volume for the same mean vertical velocity than the other UGs. After obtaining the drag coefficient using the steady-state dynamic model as described in (Anderlini et al., 2020a), it is obvious that the behaviour is caused

by a much greater drag coefficient (approximately 0.3 as compared with 0.15). After a closer inspection, both devices are found to be ocean microstructure gliders (OMG) equipped with Rockland Scientific turbulence sensors.

– For units 304 and 436, wing loss is clearly recognisable as a sudden event after 57.6 and 24.5 days from the start of the deployment, respectively. In particular, from Fig. 11, it is possible to recognise that Slocum 304 has lost the right wing, while Slocum 436 has lost its left wing as described in (Anderlini et al., 2020a). In Fig. 9, Slocum 436 presents further clear changes in the mean vertical velocity, VBD volume and roll angle at some point after failure, which is probably caused by the pilot to match a new mission objective. Additionally, after the loss of the wing, both units 304 and 436 either present higher upwards vertical velocity in ascents for the same VBD setting or a lower VBD volume for the same vertical velocity and vice versa in descents. In particular, the VBD needs to be fully retracted to enable the glider to dive. This behaviour is caused by the increase in positive buoyancy due to the wing loss.

4.2. Data Selection

After the analysis of the averaged signals and the parameters of the dynamic model, the deployments have been subdivided into training and validation datasets as shown in Table 3. The table also summarises the status of the UG during the deployment. Hence, it is clear that only healthy baseline deployments have been used in the training set, with the test subset used to assess the methods' accuracy on the baseline data. The validation datasets are used to assess the ability of the anomaly detection schemes to detect previously unseen anomalies on new real UG deployments..

Additionally, Fig. 12 shows the subdivision of the dataset into each category of glider status for the cleaned data points. As can be seen, the dataset is unbalanced and skewed towards healthy baseline operations. This is common for condition monitoring problems, where engineering systems are designed to have high reliability (Fink et al., 2020). As the anomaly detection system presented here is based on unsupervised learning solutions that are trained only from healthy baseline gliders, the methods are not negatively impacted by the imbalance. Conversely, the limited data corresponding to anomalous

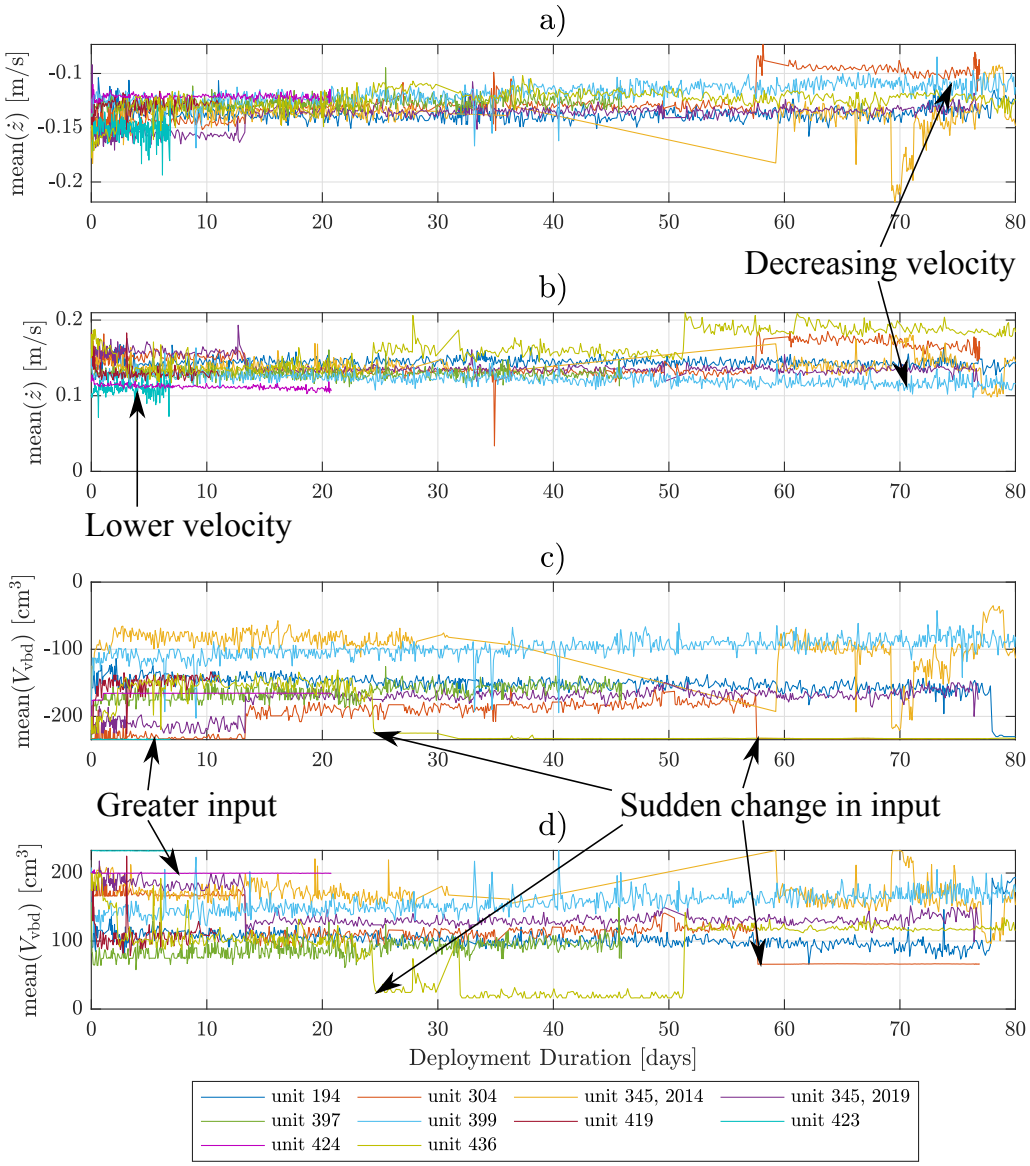

Figure 9: Mean vertical velocity and VBD volume in dives (a,c) and climbs (b,d), respectively.

behaviour will pose significant challenges for future fault diagnostics studies relying on a classification task.

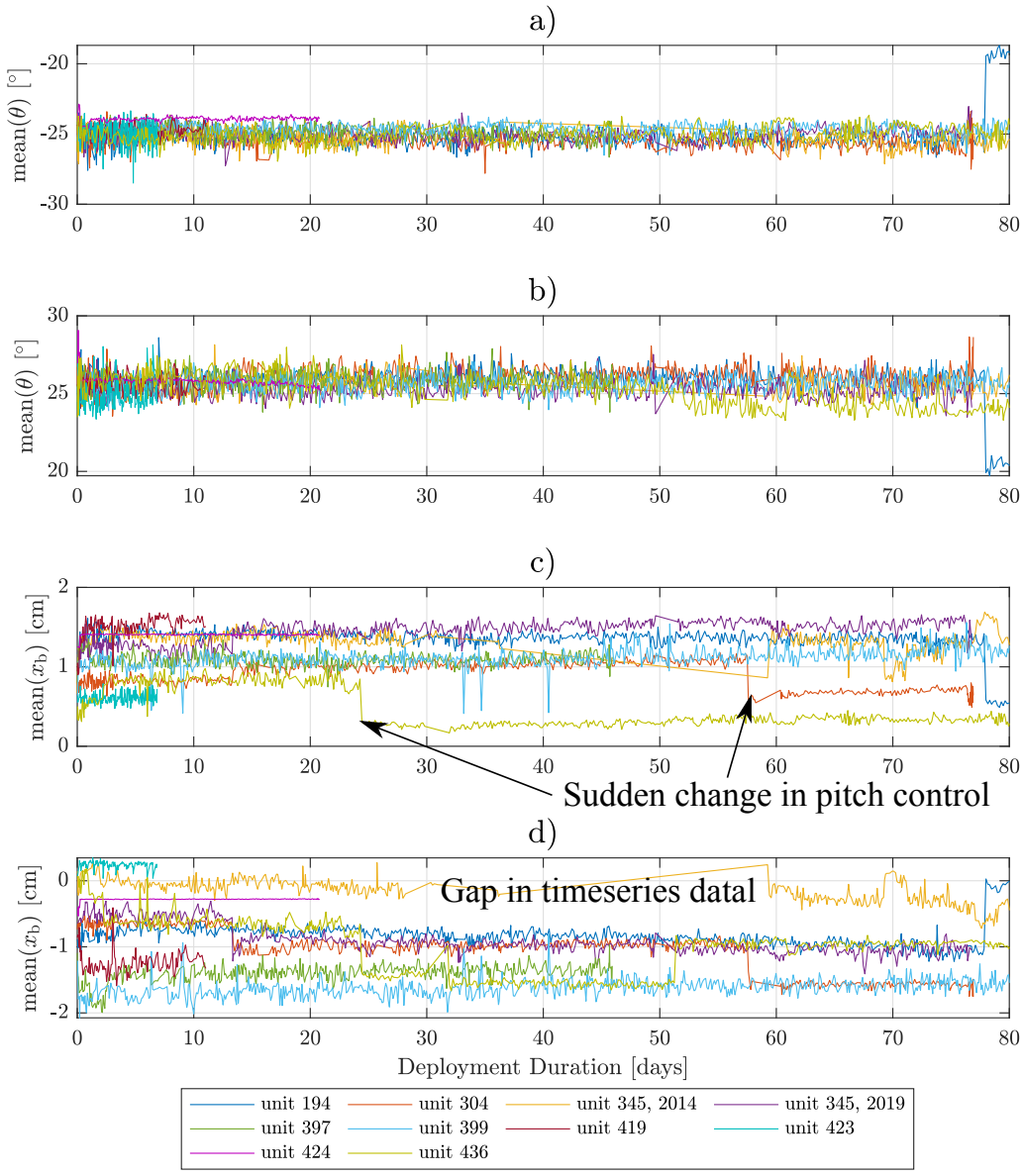

Figure 10: Mean pitch angle and battery position in dives (a,c) and climbs (b,d), respectively.

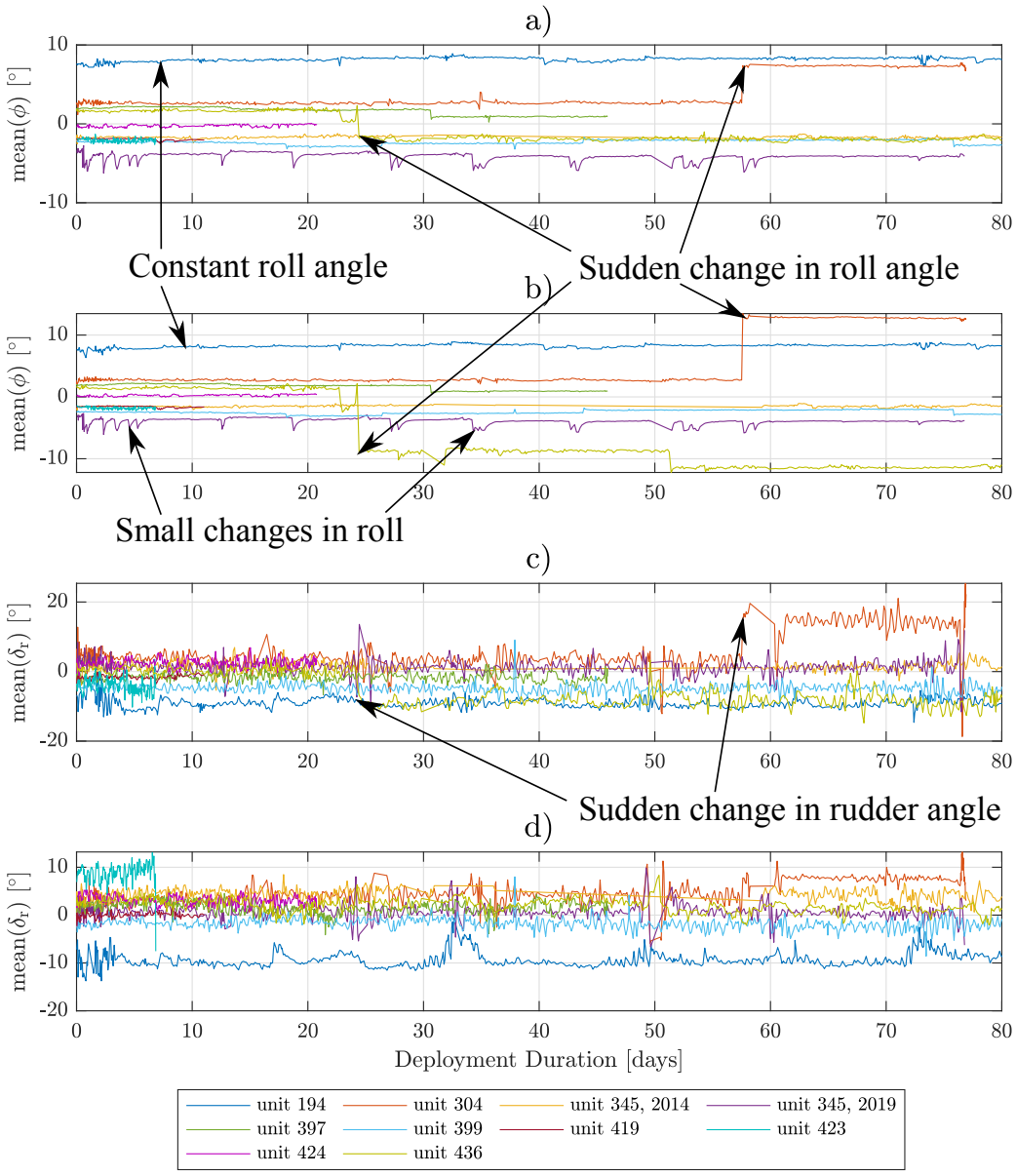

Figure 11: Mean roll and rudder angles in dives (a,c) and climbs (b,d), respectively.

4.3. Anomaly Detection Results

From hyperparameter optimisation, three hidden layers with eight neurons each are selected for the ANN and four hidden layers with twelve neurons

Table 3: Subdivision of the deployments into training (further subdivided into training, holdout and test subsets) and validation data sets.

No.	Unit	Status	Dataset	No. points
1	345	healthy	training	380,236
2	345	strong disturbances	training	325,279
3	397	healthy	training	287,139
4	419	healthy	training	68,615
5	194	angle of list	validation	492,585
6	399	possible biofouling	validation	592,680
7	423	OMG	validation	22,400
8	424	OMG	validation	122,366
9	304	wing loss	validation	275,103
10	436	wing loss	validation	555,774

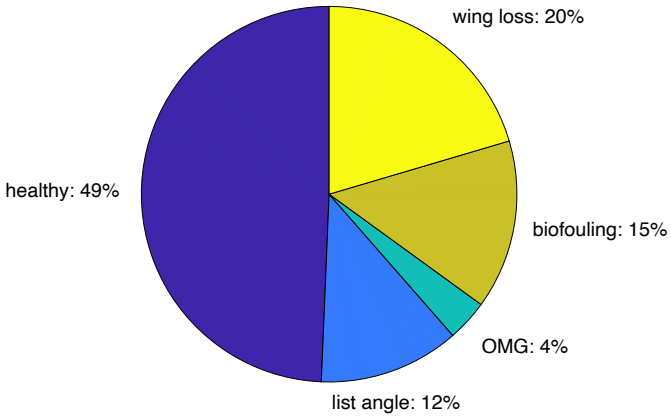

Figure 12: Share of the cleaned dataset corresponding to different types of glider behaviour. The total number of points after cleaning is 4,067,957.

each for the DNN. The PCA returned percentage total variance of 95.59%, 3.25%, 0.93% and 0.24% for the first four principal components for healthy baseline gliders. Hence, two neurons are selected for the hidden layer of the autoencoder.

For the ANN, the Wilcoxon signed rank test on the RMSE in the test set with and without f_2 presents a probability of $5.3 \times 10^{-7} \ll 0.05$. Hence, adding the feature results in a significant change. Similarly, the Lilliefors test results in a probability of $0.001 \ll 0.05$, so that the data is not normally

distributed.

The algorithms are implemented in MATLAB using the Deep Learning toolbox, selecting the default settings for training. Due to the large dataset, a minimum batch size of 512 were selected and four epochs were found to be sufficient for convergence for the ANN and DNN (corresponding to approximately 10,400 steps) and five for the autoencoder (corresponding to approximately 12,800 steps).

Fig. 13 shows the time variation of the RMSE of the trained deep learning solutions for the six test datasets selected in Table 3. In this work, the RMSE of the data-driven methods represents the anomaly score that can be used to inform classification algorithms for fault diagnostics in the future; hence, accuracy values will not be presented. Additionally, for units 304 and 436 the rule- and model-based measures to detect wing loss from Anderlini et al. (2020a) are included, namely the difference in the mean roll angle in ascents and descents and the buoyancy offset, respectively. For unit 399, the drag coefficient is the model-based metric to detect marine growth as in Anderlini et al. (2020b).

As can be seen in Fig. 13, all methods are effective in detecting wing loss for units 304 and 436. In particular, all schemes present a clear separation from the initial healthy baseline conditions and a sudden increase in the anomaly detection metric after the event, even though the RMSE of the autoencoder presents a more clearly defined change than that of the ANN and DNN. For the initial dives, the anomaly detection metrics present significant oscillations, as these are shallow, highly dynamic dives.

For unit 399, the autoencoder RMSE and the drag coefficient are the clearest indicators of growing levels of biofouling. Conversely, the RMSE of the ANN and DNN do not grow significantly.

The mean and standard deviation of the anomaly score for the three methods for the different anomalies can be seen in Table 4. The wing loss data in the table has been split before and after the event. Note that the absolute magnitude of the anomaly score is not important and varies with the method; conversely, the relative change in anomaly score between anomalous UGs and the healthy baseline is critical.

For units 194 (angle of list) and 424 (OMG), the mean anomaly score is not dissimilar from the mean values for the baseline value. This indicates that without the roll sensor input, the data-driven methods struggle to detect an angle of list, as it does not negatively impact the dynamics of the UG. Additionally, while the methods are able to generalise well to higher drag

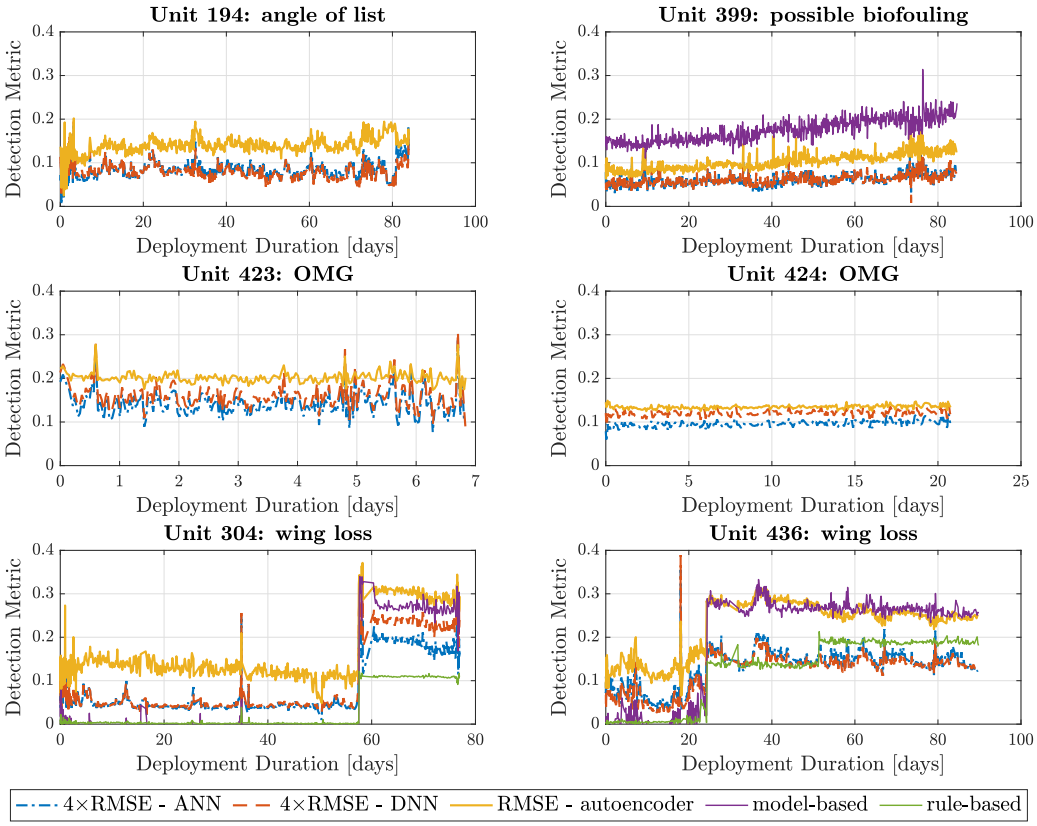

Figure 13: Anomaly detection metrics from the ANN, DNN and autoencoder for the six verification deployments. The model-based metric is the buoyancy offset (divided by 4) [N] and the rule-based metric the difference between the mean roll angle in ascents and descents (divided by 50) [°] for units 304 and 436 and the drag coefficient for unit 399.

levels caused by large appendages for the OMG unit 424, the anomaly detection metric are higher by 30%-50% than for the baseline for unit 423. The much shorter deployment for unit 423 hints at possible problems, but further investigation is required to confirm the ability of the methods to generalise to different platforms.

It is clear that the autoencoder and deep learning methods are more general than the bespoke rule- or model-based heuristics and can help detect a good range of anomalies. In particular, the dynamic model is specific to Slocum UGs, especially the model for the compressibility and thermal expansivity of its hull, and even differs from other UGs, like Seaglider UGs

Table 4: Mean (μ) and standard deviation (σ) of the anomaly score for each data-driven method for the analysed subsets. Note that only the test set has been used for the training data. The wing loss data has been split before and after the event.

Unit	**Status**	μ_{ANN}	σ_{ANN}	μ_{DNN}	σ_{DNN}	μ_{auto}	σ_{auto}
345, 397, 419	healthy	0.0137	0.0127	0.0131	0.0120	0.0978	0.0422
194	angle of list	0.0210	0.0047	0.0201	0.0045	0.1399	0.0193
399	biofouling	0.0154	0.0035	0.0153	0.0033	0.1031	0.0185
423	OMG	0.0358	0.0075	0.0401	0.0075	0.2020	0.0138
424	OMG	0.0241	0.0020	0.0302	0.0018	0.1347	0.0045
304	healthy	0.0119	0.0041	0.0127	0.0049	0.1274	0.0229
304	wing loss	0.0465	0.0055	0.0589	0.0050	0.2981	0.0194
436	healthy	0.0191	0.0081	0.0160	0.0083	0.1334	0.0263
436	wing loss	0.0384	0.0049	0.0364	0.0040	0.2630	0.0205

as described in Anderlini et al. (2019a), let alone other MAS technologies. Hence, the autoencoder is the most promising method for the fault detection of UGs thanks to its generality and superior performance in detecting wing loss clearly over the ANN and DNN.

However, the detection of some anomalies, like the angle of list, would need the inclusion of additional sensory or virtual signals, e.g. the angle of roll. As the roll sensor is non-critical for the operation of the UG, the roll signal is seldom sent to shore via satellite from operators. Hence, changes in operational practices may be required for a fuller anomaly detection system. Finally, the similar performance of the ANN and DNN methods indicates that high effort in feature engineering is not necessary when the dataset is large.

5. Conclusions

Increasing the use of MAS over the horizon requires on-line remote anomaly detection, since adverse behaviour may result in the loss of the vehicle or represent risk to other sea users. Currently, vehicles are monitored by expert pilots, thus limiting the scale of fleets of MAS that may be deployed simultaneously. In this study, different data-driven solutions including feedforward DNN and autoencoders have been introduced that are able to successfully detect a range of anomalies, including wing loss and marine growth. The data-driven methods are more general than physics-induced bespoke heuristics of rule- and model-based solutions, and are able to generalise to different

sensor configurations for UGs, including OMG. The autoencoder RMSE provided the clearest indicator for wing loss, while the change in the ANN and DNN RMSE after the sudden event was detectable, but not as clear.

In this work the fault detection system was developed off-line using data collected over past field experiments. The system is being incorporated within the NOC's command and control architecture for MAS over the horizon. Hence, it will provide remote, on-line condition monitoring of MAS during future deployments. The inclusion of additional signals and the consideration of dynamic effects will be key to extend the system to the detection of additional anomalies, e.g. angle of list and sensor loss. Field tests will need to be undertaken to collect data for additional anomalies to fully validate the efficacy and generality of the data-driven solutions. Furthermore, anomaly detection will need to be extended into full fault diagnostics to identify the affected subsystems.

Acknowledgements

The authors would like to thank Stephen Woodward, an expert glider pilot at the NOC, for his help during the collaborative project.

The research has been funded by the Lloyds Register Foundation International Programme at the Univerisity of York as part of demonstrator project "Assuring Long-term Autonomy through Detection and Diagnosis of Irregularities in Normal operation (ALADDIN)". C. A. Harris, G. Salavasidis, A. Lorenzo Lopez and A. B. Phillips' contributions are also funded under the NERC/ISCF Oceanids programme. Glider deployments analysed in this work where funded by the UK's Natural Environment Research Council (NERC) under the Altereco Project (NE/P013902/2) and CaNDyFloSS: Carbon and Nutrient Dynamics and Fluxes over Shelf Systems (NE/K001701/1).

References

Anderlini, E., Harris, C., Phillips, A.B., Lorenzo Lopez, A., Woo, M., Thomas, G., 2019a. Towards autonomy: A recommender system for the determination of trim and flight parameters for Seagliders. Ocean Engineering 189, 106338. doi:10.1016/j.oceaneng.2019.106338.

Anderlini, E., Harris, C., Woo, M., Thomas, G., 2019b. A New Recommender System for Determining Trim and Flight Parameters of Seagliders, in: 29th

International Symposium on Ocean and Polar Engineering, ISOPE, Honolulu, HI.

Anderlini, E., Harris, C.A., Salavasidis, G., Lorenzo, A., Phillips, A.B., Thomas, G., 2020a. Autonomous Detection of the Loss of a Wing for Underwater Gliders, in: IEEE/OES Autonomous Underwater Vehicle Symposium (AUV), IEEE/OES, St John's, NF, Canada. doi:10.1109/AUV50043.2020.9267895.

Anderlini, E., Real-Arce, D.A., Morales, T., Barrera, C., Hernandez-Brito, J.J., Phillips, A.B., Thomas, G., 2021. A Marine Growth Detection System for Underwater Gliders. IEEE Journal of Oceanic Engineering , 1–15doi:10.1109/JOE.2021.3066373.

Anderlini, E., Thomas, G., Woodward, S.C.A., Real-Arce, D.A., Morales, T., Barrera, C., Hernández-Brito, J.J., 2020b. Identification of the Dynamics of Biofouled Underwater Gliders, in: IEEE/OES Autonomous Underwater Vehicle Symposium (AUV), IEEE/OES, St John's, NF, Canada. doi:10.1109/AUV50043.2020.9267919.

BODC, 2021. Glider inventory. URL: https://www.bodc.ac.uk/data/bodc_database/gliders/.

Brito, M., Smeed, D., Griffiths, G., 2014. Underwater glider reliability and implications for survey design. Journal of Atmospheric and Oceanic Technology 31, 2858–2870. doi:10.1175/JTECH-D-13-00138.1.

Davis, R., Eriksen, C., Jones, C., 2003. Autonomous Buoyancy-Driven Underwater Gliders, in: Griffiths, G. (Ed.), Technology and Applications of Autonomous Underwater Vehicles. Taylor Francis, London, pp. 37–52. doi:10.1201/9780203522301.ch3.

Ellefsen, A.L., Asoy, V., Ushakov, S., Zhang, H., 2019. A comprehensive survey of prognostics and health management based on deep learning for autonomous ships. IEEE Transactions on Reliability 68, 720–740. doi:10.1109/TR.2019.2907402.

Farley, J., Morris, A.W., Jones, O.D., Harris, C.A., Lorenzo, A., 2019. Marine Science from an Armchair: A Unified Piloting Framework for Autonomous Marine Vehicles, in: IEEE Oceans, Marseille, France. pp. 1–10.

Fink, O., Wang, Q., Svensén, M., Dersin, P., Lee, W.J., Ducoffe, M., 2020. Potential, challenges and future directions for deep learning in prognostics and health management applications. Engineering Applications of Artificial Intelligence 92. doi:10.1016/j.engappai.2020.103678, arXiv:2005.02144.

Frajka-Williams, E., Eriksen, C.C., Rhines, P.B., Harcourt, R.R., 2011. Determining vertical water velocities from Seaglider. Journal of Atmospheric and Oceanic Technology 28, 1641–1656. doi:10.1175/2011JTECHO830.1.

Freddi, A., Longhi, S., Monteriù, A., 2013. Actuator fault detection system for a remotely operated vehicle, in: IFAC Proceedings Volumes (IFAC-PapersOnline), IFAC Secretariat. pp. 356–361. doi:10.3182/20130918-4-JP-3022.00050.

Gibbons, J.D., Chakraborti, S., 2011. Nonparametric Statistical Inference. 5th editio ed., Chapman Hall/CRC Press.

Goodfellow, I., Bengio, Y., Courville, A., 2016. Deep Learning. MIT Press.

Haldeman, C.D.I., Aragon, D.K., Miles, T., Scott M. Glenn, Ramos, A.G., 2016. Lessening biofouling on long-duration AUV flights: Behavior modifications and lessons learned, in: MTS/IEEE Oceans, MTS/IEEE, Monterey, California, USA. doi:10.1109/OCEANS.2016.7761236.

Hamilton, K., Lane, D.M., Brown, K.E., Evans, J., Taylor, N.K., 2007. An integrated diagnostic architecture for autonomous underwater vehicles. Journal of Field Robotics 24, 497–526. doi:10.1002/rob.20202.

Harris, C., Lorenzo, A., Jones, O., Buck, J., Kokkinaki, A., Loch, S., Gardner, T., Phillips., A.B., 2020. Oceanids C2: An integrated command,control and data infrastructure for the over-the-horizon operation of marine autonomous systems. Frontiers in Marine Science .

Jollife, I.T., Cadima, J., 2016. Principal component analysis: A review and recent developments. doi:10.1098/rsta.2015.0202.

Kingma, D.P., Ba, J.L., 2015. Adam: A Method for Stochastic Optimization, in: ICLR, San Diego, USA. URL: http://arxiv.org/abs/1412.6980, arXiv:1412.6980.

LeCun, Y., Bengio, Y., Hinton, G., 2015. Deep learning. Nature 521, 436–444. doi:10.1038/nature14539, arXiv:arXiv:1312.6184v5.

Madureira, L., Sousa, A., Braga, J., Calado, P., Dias, P., Martins, R., Pinto, J., Sousa, J., 2013. The light autonomous underwater vehicle: Evolutions and networking, in: MTS/IEEE Oceans, Bergen, Norway. doi:10.1109/OCEANS-Bergen.2013.6608189.

Matthew R. Palmer, Williams, C., Akpinar, A., Mahaffey, C., Hull, T., Toberman, M., 2020. AlterEco: An Alternative Framework to Assess Marine Ecosystem Functioning in Shelf Seas. URL: https://meetingorganizer.copernicus.org/EGU2020/EGU2020-18354.html, doi:https://doi.org/10.5194/egusphere-egu2020-18354.

McDougall, T., Barker, P., 2011. Getting started with TEOS-10 and the Gibbs Seawater (GSW) Oceanographic Toolbox. SCOR/IAPSO WG 127 , 28.

Merckelbach, L., Berger, A., Krahmann, G., Dengler, M., Carpenter, J.R., 2019. A dynamic flight model for Slocum gliders and implications for turbulence microstructure measurements. Journal of Atmospheric and Oceanic Technology 36, 281–296. doi:10.1175/jtech-d-18-0168.1.

Palmer, M.R., Williams, C., Submission, K.H., 2018. Synoptic Multi-Variable Multi-Glider Study. Technical Report.

Pang, G., Shen, C., Cao, L., Hengel, A.V.D., 2021. Deep Learning for Anomaly Detection: A Review. ACM Computing Surveys 54. doi:10.1145/3439950, arXiv:2007.02500.

Pinto, J., Dias, P.S., Martins, R., Fortuna, J., Marques, E., Sousa, J., 2013. The LSTS toolchain for networked vehicle systems, in: MTS/IEEE (Ed.), MTS/IEEE Oceans, Bergen, Norway. doi:10.1109/OCEANS-Bergen.2013.6608148.

Raanan, B.Y., Bellingham, J., Zhang, Y., Kemp, M., Kieft, B., Singh, H., Girdhar, Y., 2018. Detection of unanticipated faults for autonomous underwater vehicles using online topic models. Journal of Field Robotics 35, 705–716. doi:10.1002/rob.21771.

Reddy, K.K., Sarkar, S., Venugopalan, V., Giering, M., 2016. Anomaly Detection and Fault Disambiguation in Large Flight Data: A Multi-modal Deep Auto-encoder Approach, in: Annual Conference of the Prognostics and Health Management Society, p. 7.

Rudnick, D.L., 2016. Ocean Research Enabled by Underwater Gliders. Annual Review of Marine Science 8, 519–541. doi:10.1146/annurev-marine-122414-033913.

Schofield, O., Kohut, J., Aragon, D., Creed, L., Graver, J., Haldeman, C., Kerfoot, J., Roarty, H., Jones, C., Webb, D., Glenn, S., 2007. Slocum Gliders: Robust and ready. Journal of Field Robotics 24, 474–485. doi:10.1002/rob.20200, arXiv:10.1.1.91.5767.

Sousa Dias, P., Gomes, R.M.F., Pinto, J., Loureiro Fraga, S., Gocalves, G.M., Borges Sousa, J., Lobo Pereira, F., 2005. Neptus-A Framework to Support Multiple Vehicle Operation, in: IEEE/MTS Oceans Europe, Brest, France.

Sun, Y.S., Ran, X.R., Li, Y.M., Zhang, G.C., Zhang, Y.H., 2016. Thruster fault diagnosis method based on Gaussian particle filter for autonomous underwater vehicles. International Journal of Naval Architecture and Ocean Engineering 8, 243–251. doi:10.1016/j.ijnaoe.2016.03.003.

Teledyne Webb Research, 2012. Slocum G2 Glider Operators Manual. Technical Report. Teledyne Webb Research. URL: www.webbresearch.com.

Testor, P., DeYoung, B., Rudnick, D.L., Glenn, S., Hayes, D., Lee, C., Pattiaratchi, C.B., Hill, K.L., Heslop, E., Turpin, V., Alenius, P., Barrera, C., Barth, J., Beaird, N., Becu, G., Bosse, A., Bourrin, F., Brearley, A., Chao, Y., Chen, S., Chiggiato, J., Coppola, L., Crout, R., Cummings, J., Curry, B., Curry, R., Davis, R., Desai, K., DiMarco, S., Edwards, C., Fielding, S., Fer, I., Frajka-Williams, E., Gildor, H., Goni, G., Gutierrez, D., Hanson, S., Haugan, P., Hebert, D., Heiderich, J., Heywood, K.J., Hogan, P., Houpert, L., Huh, S., Inall, M.E., Ishii, M., ichi Ito, S., Itoh, S., Jan, S., Kaiser, J., Karstensen, J., Kirkpatrick, B., Klymak, J., Kohut, J., Krahmann, G., Krug, M., McClatchie, S., Marin, F., Mauri, E., Mehra, A., Meredith, M.P., Miles, T., Morell, J., Mortier, L., Nicholson, S., O'Callaghan, J., O'Conchubhair, D., Oke, P.R., Sanz, E.P., Palmer, M., Park, J.J., Perivoliotis, L., Poulain, P.M., Perry, R., Queste, B., Rainville,

L., Rehm, E., Roughan, M., Rome, N., Ross, T., Ruiz, S., Saba, G., Schaeffer, A., Schonau, M., Schroeder, K., Shimizu, Y., Sloyan, B.M., Smeed, D., Snowden, D.P., Song, Y., Swart, S., Tenreiro, M., Thompson, A.F., Tintore, J., Todd, R.E., Toro, C., Venables, H., Waterman, S., Watlington, R., Wilson, D., 2019. OceanGliders: A component of the integrated GOOS. doi:10.3389/fmars.2019.00422.

Thieme, C.A., Utne, I.B., 2017. Safety performance monitoring of autonomous marine systems. Reliability Engineering and System Safety 159, 264–275. doi:10.1016/j.ress.2016.11.024.

Verma, V., Simmons, R., 2006. Scalable robot fault detection and identification. Robotics and Autonomous Systems 54, 184–191. doi:10.1016/j.robot.2005.09.028.

Wang, Y., Zhang, M., 2006. Research on Test-platform and Condition Monitoring Method for AUV, in: IEEE International Conference on Mechatronics and Automation, Luoyang, China. doi:10.1109/ICMA.2006.257448.

Webb, D.C., Simonetti, P.J., Jones, C.P., 2001. SLOCUM: An underwater glider propelled by environmental energy. IEEE Journal of Oceanic Engineering doi:10.1109/48.972077.

Wood, S., 2009. Autonomous Underwater Gliders, in: Inzartsev, A. (Ed.), Underwater Vehicles. IntechOpen. chapter 26, pp. 499–524.

Yao, F., Wang, F., Zhang, M., 2018. Weak thruster fault detection for autonomous underwater vehicle based on artificial immune and signal pre-processing. Advances in Mechanical Engineering 10. doi:10.1177/1687814018758739.